Fatigue behavior of CAD-CAM composites versus lithium disilicate glass-ceramic

Yousef Karevan [a], Maher Eldafrawy [a], Raphael Herman [a],

Christelle Sanchez [a b], Michaël Sadoun [c], Amélie Mainjot [a b]

a. Dental Biomaterials Research Unit (d-BRU), Institute of Dentistry, University of Liège (ULiège), Liège, Belgium

b. Department of Fixed Prosthodontics, Institute of Dentistry, University of Liège Hospital (CHU), Liège, Belgium

c. MaJEB sprl, Liège, Belgium

Corresponding author: Amélie Mainjot. Dental Biomaterials Research Unit (d-BRU) and Department of Fixed Prosthodontics, Institute of Dentistry, University of Liège (ULiège) and University of Liège Hospital (CHU), 45 Quai G. Kurth, Liège, 4020, Belgium. e-mail: a.mainjot@chuliege.be

Acknowledgements

The authors received no financial support for this work. Dr. Michael Sadoun holds a patent (US patent 8,507,578 B2) for a composite ceramic block and is the founder of MaJEB, which contributes to the development of PICN materials. Amélie Mainjot is married to Dr. Sadoun. The authors declare no other conflict of interest with respect to the authorship and/or publication of this article.

Abstract

Objective

To assess the fatigue properties of four CAD-CAM composites and compare them with lithium disilicate glass-ceramic.

Methods

The materials studied were: Brilliant Crios (BRI); Cerasmart 270 (CER); Grandio (GRN); and Tetric CAD (TET), and a lithium disilicate glass-ceramic (IPS e.max CAD, EMX) as a reference. Blocks were cut into bars and used for: 1) 3-point flexural test (n=30/material); and 2) constructing S-N curves (n=35/material). Fatigue tests were conducted in 36°C water bath at a frequency of 1 Hz lasting up to $3x10^6$ cycles. The S-N curves were plotted using the Basquin model, assuming a distribution of fatigue life following the Weibull statistics. Digital microscopy was used to study the creep of a runout composite sample (CER), and fractured surfaces of selected samples were analyzed using laser confocal microscopy and scanning electron microscopy.

Results

Compared to EMX, CAD-CAM composites have a shorter lifespan but comparable fatigue degradation (fatigue to flexural strength ratios) at $5x10^4$ cycles (0.57-0.65 vs. 0.58). Their slow crack growth parameter (n) were close, ranging from 10.4-13.3 for CAD-CAM composites and 14.2 for EMX. Fatigue data of CAD-CAM composites showed less variability than EMX. Creep was detected in CAD-CAM composites at $3x10^6$ cycles.

Significance

Despite CAD-CAM composites having shorter lifetimes than EMX, they show similar resistance to fatigue degradation. Time-dependent factors seem to significantly influence composites fatigue at lower stress levels. Thus, extended fatigue testing in water, despite being

time-consuming and costly, is essential for understanding material behavior under clinical conditions.

Keywords: Prosthetic dentistry/prosthodontics, S-N curves, reliability, indirect composites; biomaterial(s), materials science(s); creep, IPS e.max

Introduction

The widespread adoption of CAD-CAM technology in prosthetic dentistry has opened a new venue for developing a wide range of CAD-CAM restorative materials [1]. In this context, industrial CAD-CAM composite blocks attract particular interest due to their better machinability compared to ceramics, characterized by a faster milling rate and an increased bur lifetime, a higher resistance to edge chipping and damage tolerance, and lastly an ability to be milled to extremely low thickness promoting minimally-invasive treatments [2–6]. CAD-CAM composites also have a higher damping capacity compared to ceramics [7]. Moreover, they do not require any additional firing procedures [8] and can be easily adjusted in-mouth and repaired by adding direct composite if required [9].

In comparison with light-cured direct composites, CAD-CAM composites are less operator-dependent and result in more homogeneous restorations with a higher degree of conversion. This results in lower monomer release [10] and improved mechanical properties, including better wear resistance [11], increased stiffness, and greater hardness compared to direct composites [12,13]. However, these materials have inferior mechanical properties compared to zirconia and lithium disilicate glass-ceramic materials (LDS) [14]. Attempts to overcome those shortcomings have led to the development of a variety of dispersed filler (DF) composite blocks differing in their chemical composition and microstructure [8]. DF composite blocks consists of inorganic fillers randomly dispersed within an organic matrix and polymerized at high temperatures (>100°C) [8].

It is shown that commercially available CAD-CAM composites vary in quasi-static properties [15,16]. However, while the flexural strength test is often used to compare materials as it is simple, cost-effective, and widely used in marketing, more reliable *in vitro* tests are needed to predict clinical performance. Indeed, the flexural strength test bears little resemblance to the

oral environment, where, over time, restorations fail at relatively low stress levels due to cyclic stress (i.e., chewing) combined with chemical degradation (e.g., saliva) [17,18].

A fatigue test in water can properly simulate failure due to subcritical crack growth (SCG), as seen in clinical scenarios. The combination of cyclic loading and water-induced degradation during the fatigue experiment can result in crack growth from existing flaws [19]. As a result, the material is progressively degraded until failure occurs. That is why fatigue tests are now highly recommended while performing *in vitro* studies [20].

Crack growth during fatigue commonly theoretically involves three regimes: (I) existing cracks are considered inactive; (II) cracks start to grow steadily with time (slow crack growth); and (III) crack growth becomes unstable, and the material fails in a short time. The stage II growth rate is typically estimated using the Paris power-law relationship (Eq. 1) [21]:

$$\frac{da}{dN} = C \cdot (\Delta K)^n \qquad (Eq \cdot 1)$$

where $\frac{da}{dN}$ represents the crack growth rate per cycle, ΔK denotes the amplitude of stress intensity, and the constants C and n are linked to the material and fatigue setup. The parameter 'n' determines the sensitivity of fatigue crack growth rate to the change in stress intensity ($\frac{da}{dN} \propto (\frac{K_I}{K_{IC}})^n$). If chemical degradation and/or cyclic nature of loading significantly contribute to fatigue crack growth, crack growth rate is less dependent on changes in stress level (lower 'n' value). In other words, the material with a low 'n' indicates that it is prone to fatigue degradation, and even at significantly low stress, cracks grow due to cyclic loading effects and/or chemical degradation.

Different fatigue methodologies have been used to study dental material, including the boundary methodology [22] and dynamic fatigue [23]. However, a large body of literature uses the step-stress method or the staircase approach [24], both of which are resource-efficient but provide limited insight into material behavior. The staircase method tests a material at narrowly

defined stress levels for a fixed number of cycles, so it cannot predict fatigue life across varying stresses or assess long-term performance [25]. Step-stress testing applies stresses above real-world levels and then extrapolates the results to estimate behavior at lower stresses [25]. However, that extrapolation assumes consistent material behavior across all stress ranges, which may not hold true, since, broadly, materials might exhibit different fatigue characteristics at lower stresses than at higher ones [26,27].

An alternative strategy is employing the S-N curve, which determines the number of cycles to failure at each stress level (within the investigated range). This approach is resource-demanding and less frequently used; however, according to ADM guidance on the fatigue of dental materials, it provides a more comprehensive understanding of their fatigue performance [28]. For example, it offers the advantage of examining how materials behave under different stress levels [28], and its logarithmic scale plot enables the calculation of the value of 'n' in Eq. 1 (the slope is -1/n).

Previous investigations reported that the fatigue behavior of a LDS (IPS e.max CAD, EMX; Ivoclar Vivadent, Schaan, Liechtenstein), which constitutes a reference material for single-unit prostheses, was significantly higher than Lava Ultimate [29–32]. However, to the authors' knowledge, no studies have been performed to date on the comparison between many other CAD-CAM composites and EMX through S-N curve.

Therefore, the objectives of this study were to use the S-N curve approach to compare the fatigue performance of DF CAD-CAM composites with lithium-disilicate glass-ceramic (LDS) (water bath at 36°C, and frequency of 1Hz). The null hypothesis is that the resistance to fatigue degradation ('n') does not differ significantly between EMX and CAD-CAM composites.

2. Material and methods

2.1. Materials and sample preparation

Five CAD-CAM restorative materials were studied, including four commercially available CAD-CAM composites, and one LDS. The materials, their compositions, and lot numbers are shown in Table 1. CAD-CAM blocks were cut into rectangular bars (1.6 x 4.0 x 17 ± 0.1 mm) using a low-speed saw (IsoMet; Buehler; Lake Bluff, IL, USA) under continuous water cooling. The bars were then polished on one side along their 1.6 mm thickness, sequentially with 20- and 10-µm diamond pads under running water at 150-rpm on a polishing machine (Struers; Ballerup, Denmark). Final samples thickness after polishing was around 1.5 mm, satisfying the recommended span-to-thickness ratio [33,34]. The exact dimension, however, was measured immediately before flexural strength testing with a digital caliper (Mitutoyo). Polishing of EMX was done first using 1000-grit silicon carbide paper, then with the diamond pads in the partially crystalline blue phase, following the same procedure as CAD-CAM composites. Polished EMX was then crystalized in a dedicated furnace (Programat; Ivoclar Vivadent) at 820°C for 10 s (heating rate: 90°C/min), followed by 840°C for 7 min (heating rate: 30°C/min), according to the manufacturer's recommendations. For crystallization firing, the samples were placed on the firing tray following manufacturer recommendations, i.e. using a firing paste (IPS Object Fix) to stabilize and secure them. The polished surface of samples was not in contact with this paste.

2.2. Flexural strength testing

Bars were tested in a 3-point bending device (15 mm span width), with the polished surface in tension, using a universal testing machine (Instron model 5565) controlled with software (Bluehill; Instron; Instron Canada Inc., Burlington, ON). The cross-head speed was 1 mm/min, and experimentations were conducted in ambient conditions (in air at room temperature).

Flexural strength data were not used to derive fatigue parameters directly; they were mainly used to set fatigue stress levels.

The flexural strength (FLS), σ_f, was calculated according to the following formula:

$$\text{Eq} \cdot (2) \qquad \sigma_f = \frac{3 \times F \times L}{2 \times w \times c^2}$$

Where F (N) is the load at fracture, L is the span (mm), w is the width of the specimen (mm), and c is the thickness of the specimen (mm).

2.3. Flexural fatigue testing

A total of 35 specimens per material were exposed to cyclic fatigue via a square waveform at a frequency of 1 Hz while submerged in a water bath maintained at 36°C. To prevent the specimens from slipping during the test, a minimum load of 3 N was applied. The stress level was defined to strike the best balance between providing relevant insight into the fatigue behavior of dental materials, expected to survive for many years in service, and conducting experiments within practical time and cost constraints. In this perspective, earlier studies and FLS data were used to mainly focus on high cycle fatigue life (>10^3–10^4 cycles) and allow long-term monitoring within the resource constraints [29,30,35–37].

The CAD-CAM composites were assessed at stress levels of 173 MPa (n=10/material), 152 MPa (n=10/material), 130 MPa (n=10/material) and finally 108 MPa (n=5/material). This sample size is notably larger than the typical three to five specimens used at each stress level in materials engineering [38–40]. For EMX, the stress levels were 260, 240, 220, and 200 MPa, with 10 samples tested at the higher stress levels and 5 at the lowest level (200 MPa). It is noteworthy that in addition to these 35 samples, EMX had three samples that failed before reaching the defined stress level (not included in analysis). The experiments were performed in four custom-modified fatigue machines (two Instron model 5542 and two Instron model

3304) coupled with an electromagnetic actuator (Kendrion) and Bluehill software. In addition, one more ElectroPuls E1000 (Instron) with WaveMatrix2 software was used. To prevent any potential bias, specimens from each material were evenly and randomly distributed across all fatigue machines at each stress level.

2.4. Statistical analysis of flexural strength (FLS)

Welch's ANOVA combined with Games-Howell post hoc tests were used to compare mean FLS. These tests are robust to unequal variances, in contrast to ANOVA and Tukey's post hoc test [41,42]. Tests were performed using the Pingouin [43], Statsmodels [44], and Scikit-Posthocs [45] libraries in Python (version 3.11.4, Anaconda Inc.). The Weibull analysis of the material's strength was done using ordinary linear regression with a mean rank probability function (Eqs.3 and 4). The 90% confidence intervals on Weibull parameters were established following the recommendations of Bütikofer et al. [46]. The determined parameters were used to calculate the stress levels at which 10%, 50%, and 90% of samples are expected to fail, referred to as FLS10, FLS50, and FLS90, respectively. The Weibull analysis was conducted using Microsoft Excel.

$$\text{Eq} \cdot (3) \qquad \log\left[\log\left[\frac{1}{1-\hat{F}(\sigma_i)}\right]\right] = m\log\sigma_i - m\log\sigma_0$$

$$\text{Eq} \cdot (4) \qquad \hat{F}(\sigma_i) = \left[\frac{R_i}{n+1}\right]$$

Where $F(\sigma_i)$ is failure probability, R_i is the rank of the sample with the strength of σ_i when sorted in an ascending order, and n represents the overall number of samples.

2.5. S-N curve

2.5.1 Determining life distribution at each stress level

In the present investigation, the Weibull distribution was selected to represent the fatigue lifetime at each stress level. In materials engineering, the Weibull distribution is well

established for representing scatter in materials' fatigue data, including that of composites [47,48]. The calculation of the Weibull parameter (N_0, m*) follows the method outlined in Section 2.4, but cycles to failure was used as a variable instead of FLS. The cycles to failure at 50% failure probability and the Coefficient of Variation (CV), which shows the spread of the data, were calculated for each stress level using Eqs.5 and 6 [49].

$$\text{Eq} \cdot (5) \qquad N_{50\%} = N_0 \cdot (\ln 2)^{\frac{1}{m^*}}$$

$$\text{Eq} \cdot (6) \qquad CV = \frac{\sigma}{\mu} = \sqrt{\frac{\Gamma\left(\frac{m^*+2}{m^*}\right)}{\left(\Gamma\left(\frac{m^*+1}{m^*}\right)\right)^2} - 1}$$

where Γ is the gamma function.

2.5.2 Plotting the S-N curve

Basquin model [50] was employed for plotting the S-N curve. This model is the most widely used one in the context of the S–N curve approach and applies to metals, ceramics, polymers, and composites [32,51–56]. The model assumes a power-law relationship between stress level (S) and the number of cycles to failure (N) (Eq. 7). Accordingly, a linear relationship exists between the applied stress (S) and fatigue life (N) on a logarithmic scale.

$$\text{Eq} \cdot (7) \qquad S = A \times (N)^B$$

where stress level (S) and number of cycles until failure (N) are correlated by parameters A and B.

2.5.3 Calculating the fatigue strength (FAS)

The fatigue strength (FAS) at a given number of cycles means that at this stress level and number of cycles, there is a 50% probability of failure. In other words, at a given number of cycles, 50% of the material samples have residual strength equal to or greater than the FAS at that number of cycles. The FAS was calculated using the S-N curve plots. Composites were

compared to EMX based on their FAS at 5×10^4 cycles. The composites were also compared to each other based on FAS at 2.5×10^5 cycles; these number of cycles were selected to avoid extrapolation of results.

2.5.4 Calculating the SCG parameter ('n')

The 'n' value was determined by analyzing the slope of the revised S-N curve on a logarithmic scale, where the slope equals -1/n. In the revised S-N curve, which is only used for calculating 'n' and not lifespan, data less than 10^2 cycles were excluded. This was done because 'n' is linked to steady crack growth (region II), which is difficult to assume it exists in samples that failed less than 10^2 cycles [57]. The confidence interval of regression line was calculated according to Eq. 8 [58].

$$(\mathrm{Eq}\cdot 8) \qquad 90\%\ \mathrm{CI\ (slope)} = \mathrm{slope} \pm t_{\frac{\alpha}{2}} \cdot \sqrt{\frac{\frac{\sum(y_i - \hat{y}_i)^2}{n-2}}{\sum(x_i - \bar{x})^2}}$$

where CI is the confidence interval for the slope, $t_{(\alpha/2)}$ is the critical value from the t-distribution corresponding to the desired confidence level (90%) and degrees of freedom (n– 2, where n is the number of observations), and the square root term is standard error of slope. In this equation, y_i are the observed values of the dependent variable, $\hat{y}_i$ are the predicted values from the regression line, x_i and $\bar{x}$ represent the individual and mean values of the independent variable.

2.6. Microscopy analysis:

Following fatigue testing, representative failed samples (at 108 MPa) of TET and BRI sample were examined by stitching images recorded using a laser microscope (VK-X3050, Keyence, Chicago, IL, USA; 50×). Then, the samples were analyzed by scanning electron microscopy (SEM; S-3000N, Hitachi, Tokyo, Japan) with magnification ranging from 300 to 2500X.

Results

Significant differences in mean FLS of materials were observed (Welch's ANOVA, $P < 0.001$). EMX had significantly higher mean FLS than all of the tested CAD-CAM composites. Among the four CAD-CAM composites, GRN stood out with the highest value, TET with the lowest, while BRI and CER showed no significant difference (Table 2). Moreover, it was found that the gap between the strength of EMX and composites was reduced at lower failure probabilities and increased at higher failure probabilities. The EMX Weibull modulus was significantly lower than that of TET and GRN, but there was no significant difference between EMX, BRI, and CER.

Table 3 provides the Weibull distribution parameters for different stress levels, which were utilized in constructing the S-N curves. The S-N experimental curves, displayed in Fig. 1, were used to obtain information regarding the fatigue life of each material (Section 2.5.2).

CAD-CAM composites generally seemed to have a higher fatigue strength (FAS)-to-FLS ratio at $5x10^4$ cycles compared to EMX, and only GRN had a similar ratio. The FAS of composites ranged from 121 to 108 MPa, which fell within the range of 49% to 56% of their FLS. The 'n' varied between 10.4 and 14.2, with EMX having the highest value and TET having the lowest. However, because the confidence interval of the 'n' value of CAD-CAM composites encompassed the point estimate of EMX (14.2), they were statistically the same [59]. A similar argument is valid when comparing composites (Table 4).

One of the CAD-CAM composites reached runout (CER at 108 MPa), which showed time-dependent plastic deformation during the fatigue test. After two months, a portion of this plastic deformation was recovered, however, some permanent plastic deformation persisted in the material (creep; Fig. 2).

Fig. 3 shows the fracture surface analysis of two failed samples at low-stress levels. In Fig. 3A, a large flaw leads to a sample fracture (the TET sample failed near 10^5 cycles). In Figs. 3B1

and 3B2, the presence of a large flaw and the formation of micro-cracks near the surface in tension is depicted, respectively (the BRI sample survived more than $9x10^5$ cycles at 108 MPa). When comparing the reliability of materials, EMX showed a higher scatter of fatigue data compared to the composites, as evidenced by its higher CV in Fig. 4. Among CAD-CAM composites, CV of GRN was comparatively low and stable. However, for the remaining CAD-CAM composites, a decrease in stress levels leads to a reduction in CV (Fig. 4).

Discussion

The fatigue behavior of CAD–CAM materials was studied using the S–N curve method (3-point flexural setup). Tests were conducted using 1 Hz frequency as lower bound of human chewing frequency (mean 1.57 Hz; range 0.94–2.15 Hz (5th–95th percentile)) [60], in distilled water, and extended up to $3x10^6$ cycles. To avoid extrapolation, the FAS/FLS of composites and EMX was compared at $5x10^4$ cycles, and composite FAS was analyzed at $2.5x10^5$ cycles.

EMX had a longer lifetime compared to CAD-CAM composites. However, fatigue resistance of CAD-CAM composites is comparable to that of EMX; and the scatter of their fatigue data is less than that of EMX, indicating their higher reliability. Interestingly, it seems that the fatigue behavior of CAD-CAM composites, specifically those with higher polymer content, including CER, TET, and BRI (Table 1), significantly varies depending on stress levels (Fig. 4).

Two pieces of evidence show that CAD-CAM composites and EMX have comparable fatigue sensitivity. Firstly, similar FAS/FLS at $5x10^4$ cycles; secondly, comparable SCG parameter ('n') between CAD-CAM composites and EMX. As it can be seen in Table 4, the SCG resistance of EMX, despite being a ceramic (ceramics typically have 'n' values ranging from 10 to 100 [21]), is similar to that of CAD-CAM composites (polymers have typical 'n' values

below 10 [21]). One reason can be the degradation of the "bridging" mechanism in EMX, which can happen after a short interval of cyclic loading [61,62]. Indeed, it is known that in the absence of cyclic loading, the intact crystals at the wake of an advancing crack act as bridges (in EMX the cracks propagate through glass phase [63]). Therefore, they are restricting the crack opening until sufficient energy is reached to overcome the friction between the crystals and the crack walls. This energy-consuming mechanism plays a role in high fracture toughness and strength of LDS [62,64,65]. However, broadly, during cyclic loading, the repeated relative motion of crystals and crack walls can crush the asperities, greatly diminish friction, and degrade the bridging mechanism [51,66]. The second reason can be the dissolution of one of the phases, because high fatigue sensitivity of EMX is also reported by Liu et al. [67] in the dynamic fatigue test (in the absence of cyclic loading). Of note, similar to composites examined here, Lava Ultimate also had higher fatigue resistance compared to EMX [29–31].

On the other hand, one advantage of CAD-CAM composites over EMX is their lower data scatter, implying higher reliability. The high scatter of data in EMX can possibly be justified by the large difference in strength of the samples (Table 2). According to the widely accepted assumption of equal ranks, if samples of a material are ranked by strength, their fatigue life will follow a similar ranking. Therefore, for example, the first failed sample at 220 MPa corresponds to ~249 MPa (~88% of FLS10 in Table 2; failed after ~5 cycles). However, the runout sample is corresponding to ~462 MPa (~47% of FLS90 in Table 2; did not fail after $3x10^6$ cycles). The high scatter of fatigue data for EMX is common and has been observed in other studies [29,32]. For example, it can be interpreted from the study by Kristen et al. [61], where they found the Weibull modulus of less than one. Moreover, there was a runout of $2.5x10^6$ cycles, while the lifetime at a 63.3% failure probability was much shorter at about $8x10^3$ cycles [68].

This justification is particularly relevant for ceramics, as flaws have a paramount importance in strength and fatigue behavior (or in the case of CAD-CAM composites fatigue behaviors under high stress). However, at lower stress levels, the fatigue behavior of composites became significantly more complex, and several factors, besides flaws (Fig. 3A and 3B1), contribute to the fatigue performance of CAD-CAM composites including creep (Fig. 2), micro-crack formation (Fig. 3B2), water degradation, and silane hydrolysis. Fig. 3 illustrates that these phenomena can occur together within a single sample during fatigue testing. The positive effects of water sorption or creep on the fatigue behavior of polymer composites have been proposed in some studies [69,70], while their negative impacts are documented in others [71,72]. These contradictory outcomes might stem in testing conditions, material composition, and the duration of fatigue life.

The influence of time-dependent phenomena such as water sorption and creep might be the reason behind lower scatter of fatigue data at lower stresses. In this context, GRN showed relatively consistent CV values under both high and low stress conditions (Fig. 4). Similarly, Wendler et al. [72] observed that the 'n' values of GRN did not change significantly before and after aging, unlike other composites. These observations might attribute to this fact that GRN is less affected by water sorption and creep deformation because of its higher filler content.

The provided explanations highlight the importance of time-dependent phenomena on fatigue behavior. Therefore, it can be recommended that if resource constraints necessitate an accelerated fatigue test, it is important to adhere to the recommendation in ref. [25] and not extrapolate beyond 4 times the test duration when estimating survival time at a lower stress level.

Acknowledging that uncertainty is inherent in fatigue studies, the future aim of this study is to reduce the uncertainty of findings. The uncertainty can stem from different factors, including

uncertainty of statistical analysis and the interblock variability of CAD-CAM materials, where subtle variations in block properties can affect fatigue performance. While increasing the number of tested samples is a potential solution, it may not be practical to collect more than 35 samples used in the present study due to the extended testing time required at low stress levels, with each runout sample taking approximately five weeks. Therefore, alternative solutions, such as using different test setups, e.g., four-point bending, could be explored in future studies. This approach subjects a larger volume of material to the maximum calculated stress level, making each sample more representative of the material's properties.

Additionally, it could be interesting to compare fatigue performance of materials not only based on the S-N curve, but also based on strain–lifetime relation (ε-N curve); which might favorably impact the performance of CAD-CAM composites compared to EMX. The reason that the S-N curve alone may not suffice is that Duan et al. showed that materials with different elastic modulus can exhibit significant variations in maximum stress level and stress distribution, even under identical loading conditions (e.g., chewing force) [73]. Finally, it would be worthwhile to evaluate more advanced fatigue-life models and compare their predictive performance with that of the Basquin model.

5. Conclusion

The fatigue lifetime of CAD-CAM composites was inferior to that of EMX, but their resistance to fatigue degradation (subcritical crack growth; 'n') was comparable. No CAD-CAM composites were significantly better or worse than the others.

Several factors affect the fatigue behavior of CAD-CAM materials over long periods, which cannot be fully addressed under quasi-static conditions or short-term fatigue tests. This study demonstrates that, over time, the lifetime of CAD-CAM composites is influenced not only by flaws, but also by factors such as micro-cracking and creep.

To understand how time-dependent phenomena influence the behavior of CAD-CAM composites, long-term experimentation under lower stress levels that more closely resemble typical clinical conditions is needed. Therefore, even though low-frequency, long-duration fatigue tests are costly and time-consuming, they are essential for providing reliable insights into the long-term performance of CAD-CAM composites in clinical scenarios.

6. Declaration of Generative AI and AI-assisted technologies in the writing process

During the preparation of this work, the authors used ChatGPT in order to improve readability and language. After using this tool/service, the authors reviewed and edited the content as needed and take full responsibility for the content of the publication

References

[1] Marchesi G, Camurri Piloni A, Nicolin V, Turco G, Di Lenarda R. Chairside CAD/CAM Materials: Current Trends of Clinical Uses. Biology 2021;10:1170. https://doi.org/10.3390/biology10111170.

[2] Coldea A, Fischer J, Swain MV, Thiel N. Damage tolerance of indirect restorative materials (including PICN) after simulated bur adjustments. Dent Mater 2015;31:684–94. https://doi.org/10.1016/j.dental.2015.03.007.

[3] Lebon N, Tapie L, Vennat E, Mawussi B. Influence of CAD/CAM tool and material on tool wear and roughness of dental prostheses after milling. J Prosthet Dent 2015;114:236–47. https://doi.org/10.1016/j.prosdent.2014.12.021.

[4] Chavali R, Nejat AH, Lawson NC. Machinability of CAD-CAM materials. J Prosthet Dent 2017;118:194–9. https://doi.org/10.1016/j.prosdent.2016.09.022.

[5] Curran P, Cattani-Lorente M, Anselm Wiskott HW, Durual S, Scherrer SS. Grinding damage assessment for CAD-CAM restorative materials. Dent Mater 2017;33:294–308. https://doi.org/10.1016/j.dental.2016.12.004.

[6] Pfeilschifter M, Preis V, Behr M, Rosentritt M. Edge strength of CAD/CAM materials. J Dent 2018;74:95–100. https://doi.org/10.1016/j.jdent.2018.05.004.

[7] Niem Th, Gonschorek S, Wöstmann B. New method to differentiate surface damping behavior and stress absorption capacities of common CAD/CAM restorative materials. Dent Mater 2021;37:e213–30. https://doi.org/10.1016/j.dental.2020.12.012.

[8] Mainjot AK, Dupont NM, Oudkerk JC, Dewael TY, Sadoun MJ. From Artisanal to CAD-CAM Blocks: State of the Art of Indirect Composites. J Dent Res 2016;95:487–95. https://doi.org/10.1177/0022034516634286.

[9] Zaghloul H, Elkassas DW, Haridy MF. Effect of incorporation of silane in the bonding agent on the repair potential of machinable esthetic blocks. Eur J Dent 2014;08:044–52. https://doi.org/10.4103/1305-7456.126240.

[10] Mourouzis P, Andreasidou E, Samanidou V, Tolidis K. Short-term and long-term release of monomers from newly developed resin-modified ceramics and composite resin CAD-CAM blocks. J Prosthet Dent 2020;123:339–48. https://doi.org/10.1016/j.prosdent.2019.01.012.

[11] Lauvahutanon S, Takahashi H, Oki M, Arksornnukit M, Kanehira M, Finger WJ. *In vitro* evaluation of the wear resistance of composite resin blocks for CAD/CAM. Dent Mater J 2015;34:495–502. https://doi.org/10.4012/dmj.2014-293.

[12] Swain MV, Coldea A, Bilkhair A, Guess PC. Interpenetrating network ceramic-resin composite dental restorative materials. Dent Mater 2016;32:34–42. https://doi.org/10.1016/j.dental.2015.09.009.

[13] Ramos JC, Marinho A, Messias A, Almeida G, Vinagre A, Dias R. Mechanical Properties of Direct Composite Resins and CAD/CAM Composite Blocks. Oral 2024;4:206–16. https://doi.org/10.3390/oral4020017.

[14] Ruse ND, Sadoun MJ. Resin-composite Blocks for Dental CAD/CAM Applications. J Dent Res 2014;93:1232–4. https://doi.org/10.1177/0022034514553976.

[15] Grzebieluch W, Mikulewicz M, Kaczmarek U. Resin Composite Materials for Chairside CAD/CAM Restorations: A Comparison of Selected Mechanical Properties. J Healthc Eng 2021;2021:1–8. https://doi.org/10.1155/2021/8828954.

[16] Ducke VM, Ilie N. Aging behavior of high-translucent CAD/CAM resin-based composite blocks. J Mech Behav Biomed Mater 2021;115:104269. https://doi.org/10.1016/j.jmbbm.2020.104269.

[17] Lohbauer U, Belli R, Ferracane JL. Factors Involved in Mechanical Fatigue Degradation of Dental Resin Composites. J Dent Res 2013;92:584–91. https://doi.org/10.1177/0022034513490734.

[18] Ferracane JL. Hygroscopic and hydrolytic effects in dental polymer networks. Dent Mater 2006;22:211–22. https://doi.org/10.1016/j.dental.2005.05.005.

[19] Ilie N, Hilton TJ, Heintze SD, Hickel R, Watts DC, Silikas N, et al. Academy of Dental Materials guidance—Resin composites: Part I—Mechanical properties. Dent Mater 2017;33:880–94. https://doi.org/10.1016/j.dental.2017.04.013.

[20] Drummond JL. Degradation, Fatigue, and Failure of Resin Dental Composite Materials. J Dent Res 2008;87:710–9. https://doi.org/10.1177/154405910808700802.

[21] Kruzic JJ, Arsecularatne JA, Tanaka CB, Hoffman MJ, Cesar PF. Recent advances in understanding the fatigue and wear behavior of dental composites and ceramics. J Mech Behav Biomed Mater 2018;88:504–33. https://doi.org/10.1016/j.jmbbm.2018.08.008.

[22] Ottoni R, Griggs JA, Corazza PH, Della Bona Á, Borba M. Precision of different fatigue methods for predicting glass-ceramic failure. J Mech Behav Biomed Mater 2018;88:497–503. https://doi.org/10.1016/j.jmbbm.2018.09.004.

[23] Teixeira EC, Piascik JR, Stoner BR, Thompson JY. Dynamic fatigue and strength characterization of three ceramic materials. J Mater Sci Mater Med 2007;18:1219–24. https://doi.org/10.1007/s10856-007-0131-4.

[24] Velho HC, Dapieve KS, Valandro LF, Pereira GKR, Venturini AB. Cyclic fatigue tests on non-anatomic specimens of dental ceramic materials: A scoping review. J Mech Behav Biomed Mater 2022;126:104985. https://doi.org/10.1016/j.jmbbm.2021.104985.

[25] Bonfante EA, Coelho PG. A Critical Perspective on Mechanical Testing of Implants and Prostheses. Adv Dent Res 2016;28:18–27. https://doi.org/10.1177/0022034515624445.

[26] Schijve J. Fatigue of Structures and Materials. Dordrecht: Kluwer Academic Publishers; 2004. https://doi.org/10.1007/0-306-48396-3.

[27] Ansari MdTA, Singh KK, Azam MS. Fatigue damage analysis of fiber-reinforced polymer composites—A review. J Reinf Plast Compos 2018;37:636–54. https://doi.org/10.1177/0731684418754713.

[28] Kelly JR, Cesar PF, Scherrer SS, Della Bona A, van Noort R, Tholey M, et al. ADM guidance-ceramics: Fatigue principles and testing. Dent Mater 2017;33:1192–204. https://doi.org/10.1016/j.dental.2017.09.006.

[29] Wendler M, Belli R, Valladares D, Petschelt A, Lohbauer U. Chairside CAD/CAM materials. Part 3: Cyclic fatigue parameters and lifetime predictions. Dent Mater 2018;34:910–21. https://doi.org/10.1016/j.dental.2018.03.024.

[30] Belli R, Geinzer E, Muschweck A, Petschelt A, Lohbauer U. Mechanical fatigue degradation of ceramics versus resin composites for dental restorations. Dent Mater 2014;30:424–32. https://doi.org/10.1016/j.dental.2014.01.003.

[31] Ankyu S, Nakamura K, Harada A, Hong G, Kanno T, Niwano Y, et al. Fatigue analysis of computer-aided design/computer-aided manufacturing resin-based composite vs. lithium disilicate glass-ceramic. Eur J Oral Sci 2016;124:387–95. https://doi.org/10.1111/eos.12278.

[32] Homaei E, Farhangdoost K, Tsoi JKH, Matinlinna JP, Pow EHN. Static and fatigue mechanical behavior of three dental CAD/CAM ceramics. J Mech Behav Biomed Mater 2016;59:304–13. https://doi.org/10.1016/j.jmbbm.2016.01.023.

[33] International Organization for Standardization. ISO 6872: 2015. Dentistry—ceramic materials 2015.

[34] Alander P, Lassila L, Vallittu P. The span length and cross-sectional design affect values of strength. Dent Mater 2005;21:347–53. https://doi.org/10.1016/j.dental.2004.05.009.

[35] Horwood A, Chockalingam N. Principles of materials science. Clin. Biomech. Hum. Locomot., Elsevier; 2023, p. 91–174. https://doi.org/10.1016/B978-0-323-85212-8.00002-X.

[36] Pelleg J. Mechanical Properties of Ceramics. Cham: Springer; 2014. https://doi.org/10.1007/978-3-319-04492-7.

[37] Chen X, Bu J, Fan X, Lu J, Xu L. Effect of loading frequency and stress level on low cycle fatigue behavior of plain concrete in direct tension. Constr Build Mater 2017;133:367–75. https://doi.org/10.1016/j.conbuildmat.2016.12.085.

[38] Huang J, Yang H, Liu W, Zhang K, Huang A. Confidence level and reliability analysis of the fatigue life of CFRP laminates predicted based on fracture fatigue entropy. Int J Fatigue 2022;156:106659. https://doi.org/10.1016/j.ijfatigue.2021.106659.

[39] Chen J, Liu S, Zhang W, Liu Y. Uncertainty quantification of fatigue S-N curves with sparse data using hierarchical Bayesian data augmentation. Int J Fatigue 2020;134:105511. https://doi.org/10.1016/j.ijfatigue.2020.105511.

[40] Heintze SD, Monreal D, Rousson V. Fatigue resistance of denture teeth. J Mech Behav Biomed Mater 2016;53:373–83. https://doi.org/10.1016/j.jmbbm.2015.08.034.

[41] Liu H. Comparing Welch's ANOVA, a Kruskal-Wallis test and traditional ANOVA in case of Heterogeneity of Variance. Virginia Commonwealth University, 2015.

[42] Games PA, Howell JF. Pairwise Multiple Comparison Procedures with Unequal N's and/or Variances: A Monte Carlo Study. J Educ Stat 1976;1:113–25. https://doi.org/10.3102/10769986001002113.

[43] Vallat R. Pingouin: statistics in Python. J Open Source Softw 2018;3:1026. https://doi.org/10.21105/joss.01026.

[44] Seabold S, Perktold J. Statsmodels: econometric and statistical modeling with python. vol. 7, 2010.

[45] Terpilowski M. scikit-posthocs: Pairwise multiple comparison tests in Python. J Open Source Softw 2019;4:1169. https://doi.org/10.21105/joss.01169.

[46] Bütikofer L, Stawarczyk B, Roos M. Two regression methods for estimation of a two-parameter Weibull distribution for reliability of dental materials. Dent Mater 2015;31:e33–50. https://doi.org/10.1016/j.dental.2014.11.014.

[47] Xiang G, Bacharoudis KC, Vassilopoulos AP. Probabilistic fatigue model for composites based on the statistical characteristics of the cycles to failure. Int J Fatigue 2022;163:107085. https://doi.org/10.1016/j.ijfatigue.2022.107085.

[48] Qiao P, Yang M. Fatigue Life Prediction of Pultruded E-glass/Polyurethane Composites. J Compos Mater 2006;40:815–37. https://doi.org/10.1177/0021998305055549.

[49] La-ongkaew M, Niwitpong S-A, Niwitpong S. Confidence intervals for the difference between the coefficients of variation of Weibull distributions for analyzing wind speed dispersion. PeerJ 2021;9:e11676. https://doi.org/10.7717/peerj.11676.

[50] Basquin OH. The exponential law of endurance test. Soc Test Mater Proc 1910;10:625–30.

[51] Barsoum M. Fundamentals of ceramics. CRC press; 2019.

[52] Burhan I, Kim H. S-N Curve Models for Composite Materials Characterisation: An Evaluative Review. J Compos Sci 2018;2:38. https://doi.org/10.3390/jcs2030038.

[53] Chandran KSR. Mechanical fatigue of polymers: A new approach to characterize the S N behavior on the basis of macroscopic crack growth mechanism. Polymer 2016;91:222–38. https://doi.org/10.1016/j.polymer.2016.03.058.

[54] Yang M, Gao C, Pang J, Li S, Hu D, Li X, et al. High-Cycle Fatigue Behavior and Fatigue Strength Prediction of Differently Heat-Treated 35CrMo Steels. Metals 2022;12:688. https://doi.org/10.3390/met12040688.

[55] Scherrer SS, Cattani-Lorente M, Vittecoq E, De Mestral F, Griggs JA, Wiskott HWA. Fatigue behavior in water of Y-TZP zirconia ceramics after abrasion with 30μm silica-

coated alumina particles. Dent Mater 2011;27:e28–42. https://doi.org/10.1016/j.dental.2010.10.003.

[56] Arola D, Reprogel RK. Effects of aging on the mechanical behavior of human dentin. Biomaterials 2005;26:4051–61. https://doi.org/10.1016/j.biomaterials.2004.10.029.

[57] Kirane K, Bažant ZP. Size effect in Paris law and fatigue lifetimes for quasibrittle materials: Modified theory, experiments and micro-modeling. Int J Fatigue 2016;83:209–20. https://doi.org/10.1016/j.ijfatigue.2015.10.015.

[58] Schneider CRA, Maddox SJ. Best practice guide on statistical analysis of fatigue data. Granta Park, Great Abington, Cambridge, UK: 2003.

[59] Greenland S, Senn SJ, Rothman KJ, Carlin JB, Poole C, Goodman SN, et al. Statistical tests, P values, confidence intervals, and power: a guide to misinterpretations. Eur J Epidemiol 2016;31:337–50. https://doi.org/10.1007/s10654-016-0149-3.

[60] Po JMC, Kieser JA, Gallo LM, Tésenyi AJ, Herbison P, Farella M. Time-Frequency Analysis of Chewing Activity in the Natural Environment. J Dent Res 2011;90:1206–10. https://doi.org/10.1177/0022034511416669.

[61] Kirsten J, Belli R, Wendler M, Petschelt A, Hurle K, Lohbauer U. Crack growth rates in lithium disilicates with bulk (mis)alignment of the Li2Si2O5 phase in the [001] direction. J Non-Cryst Solids 2020;532:119877. https://doi.org/10.1016/j.jnoncrysol.2019.119877.

[62] Lubauer J, Lohbauer U, Belli R. Fatigue Threshold R-Curves for Dental Lithium Disilicate Glass–Ceramics. J Dent Res 2023;102:1106–13. https://doi.org/10.1177/00220345231180565.

[63] Apel E, Deubener J, Bernard A, Höland M, Müller R, Kappert H, et al. Phenomena and mechanisms of crack propagation in glass-ceramics. J Mech Behav Biomed Mater 2008;1:313–25. https://doi.org/10.1016/j.jmbbm.2007.11.005.

[64] Belli R, Wendler M, Cicconi MR, De Ligny D, Petschelt A, Werbach K, et al. Fracture anisotropy in texturized lithium disilicate glass-ceramics. J Non-Cryst Solids 2018;481:457–69. https://doi.org/10.1016/j.jnoncrysol.2017.11.040.

[65] Senk MV, Mathias I, Zanotto ED, Serbena FC. Crystallized fraction and crystal size effects on the strength and toughness of lithium disilicate glass-ceramics. J Eur Ceram Soc 2023;43:3600–9. https://doi.org/10.1016/j.jeurceramsoc.2023.02.004.

[66] Ritchie RO. Mechanisms of fatigue-crack propagation in ductile and brittle solids. Int J Fract 1999;100:55–83.

[67] Liu C, Eser A, Albrecht T, Stournari V, Felder M, Heintze S, et al. Strength characterization and lifetime prediction of dental ceramic materials. Dent Mater 2021;37:94–105. https://doi.org/10.1016/j.dental.2020.10.015.

[68] Gonzaga CC, Cesar PF, Miranda WG, Yoshimura HN. Slow crack growth and reliability of dental ceramics. Dent Mater 2011;27:394–406. https://doi.org/10.1016/j.dental.2010.10.025.

[69] Takeshige F, Kawakami Y, Hayashi M, Ebisu S. Fatigue behavior of resin composites in aqueous environments. Dent Mater 2007;23:893–9. https://doi.org/10.1016/j.dental.2006.06.031.

[70] Vaidyanathan J, Vaidyanathan TK. Flexural creep deformation and recovery in dental composites. J Dent 2001;29:545–51. https://doi.org/10.1016/S0300-5712(01)00049-5.

[71] Spathis G, Kontou E. Creep failure time prediction of polymers and polymer composites. Compos Sci Technol 2012;72:959–64. https://doi.org/10.1016/j.compscitech.2012.03.018.

[72] Wendler M, Stenger A, Ripper J, Priewich E, Belli R, Lohbauer U. Mechanical degradation of contemporary CAD/CAM resin composite materials after water ageing. Dent Mater 2021;37:1156–67. https://doi.org/10.1016/j.dental.2021.04.002.

[73] Duan Y, Griggs JA. Effect of elasticity on stress distribution in CAD/CAM dental crowns: Glass ceramic vs. polymer–matrix composite. J Dent 2015;43:742–9. https://doi.org/10.1016/j.jdent.2015.01.008.

Legends of Figures

Fig. 1. S-N curves of (A) Brilliant Crios (BRI), (B) Cerasmart 270 (CER), (C) Grandio (GRN), (D) Tetric CAD (TET), and (E) IPS e.max CAD (EMX). The purple circle in CER and EMX indicate the runout sample at $3x10^6$ cycles.

Fig. 2. Digital microscopy (20x) showing a plastic deformation of a runout sample. The red lines show two parallel lines between the support span (the initial state of samples before fatigue testing). (A) Cerasmart 270 (CER) at 108 MPa after $3x10^6$ cycles; (B) CER runout at

108 MPa after two months of recovery. Some of the of the plastic deformation seen in Fig. 2A has been recovered, but not completely.

Fig. 3. Laser confocal microscope shows an overview of the fractured surface, and the SEM analysis provides detailed information about the fractured samples. A) Tetric CAD (TET) failed at 108MPa (shortest lifetime; red circle shows the flaw that caused the failure); (B) Brilliant Crios (BRI) sample survived more than $9x10^5$ cycles with a critical flaw in the compression region (red rectangle; B1) and clear tension-side microcracks (yellow rectangle; B2).

Fig. 4. Coefficient of variation (CV) of studied materials at different stress levels, (A) CAD-CAM composites: Brilliant Crios (BRI), Cerasmart 270 (CER), Tetric CAD (TET) and Grandio blocs (GRN), and (B) IPS e.max CAD (EMX). High CV means a high scatter of fatigue life in material specimens, implying less consistent behavior of the material.

Legends of Tables

Table 1. CAD-CAM blocks used in the study and their compositions

Table 2. Statistical analysis of FLS

Table 3. The Weibull parameters for fatigue life of CAD/CAM composites and EMX at different stress levels

Table 4. FAS: fatigue strength obtained from S-N curves, FAS/FLS ratio: fatigue-to-flexural strength ratio, 'n': The SCG parameter of studied materials

FIGURE 1

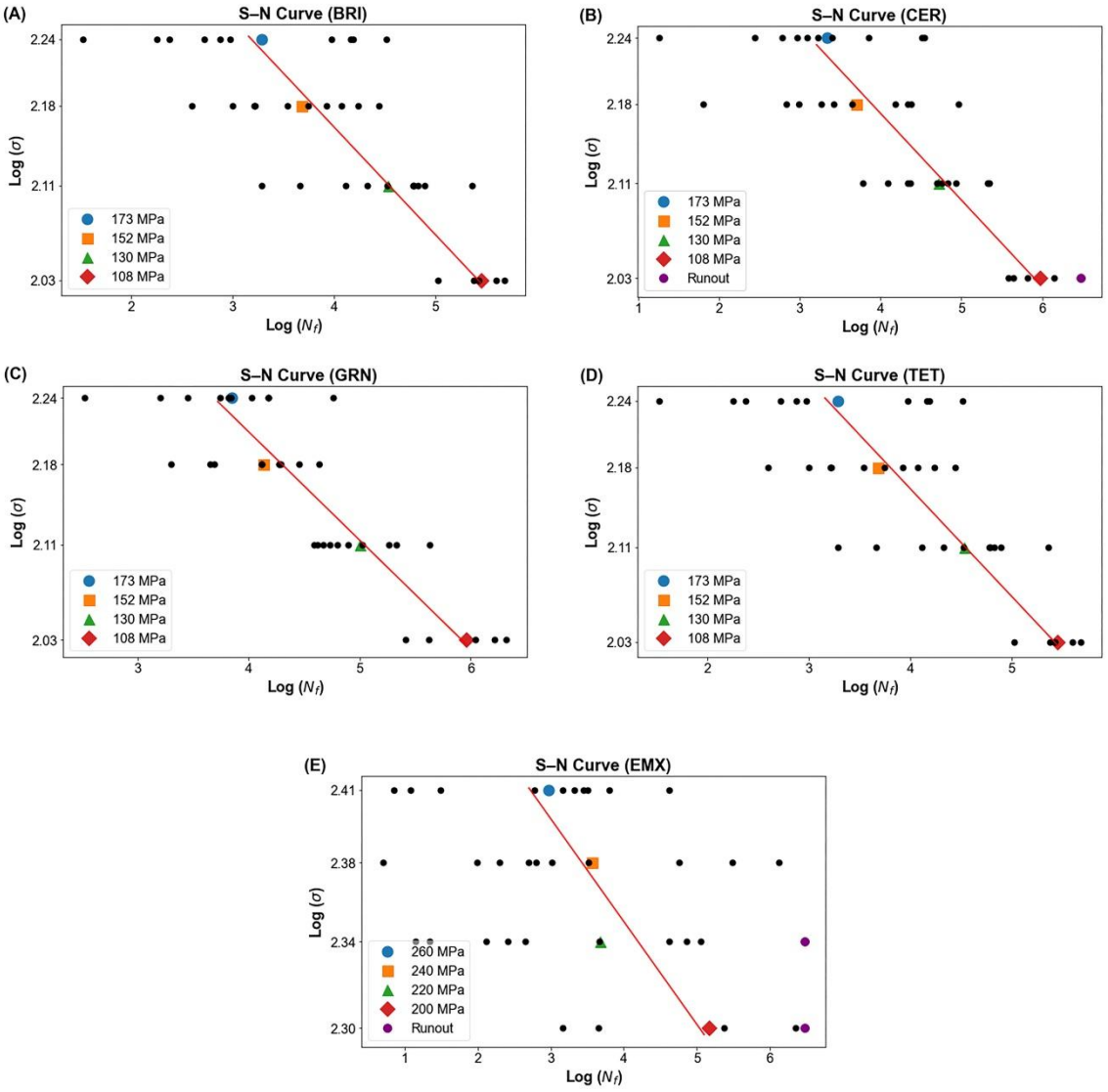
(A)
S–N Curve (BRI)
Log (σ)
Log (N_f)
173 MPa
152 MPa
130 MPa
108 MPa
(B)
S–N Curve (CER)
Log (σ)
Log (N_f)
173 MPa
152 MPa
130 MPa
108 MPa
Runout
(C)
S–N Curve (GRN)
Log (σ)
Log (N_f)
173 MPa
152 MPa
130 MPa
108 MPa
(D)
S–N Curve (TET)
Log (σ)
Log (N_f)
173 MPa
152 MPa
130 MPa
108 MPa
(E)
S–N Curve (EMX)
Log (σ)
Log (N_f)
260 MPa
240 MPa
220 MPa
200 MPa
Runout

FIGURE 2

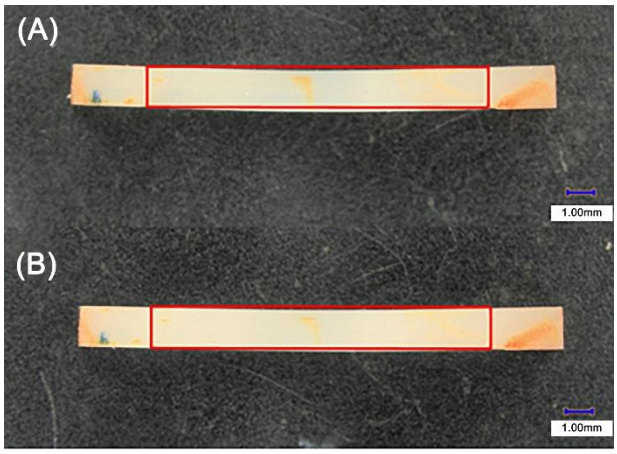

FIGURE 3

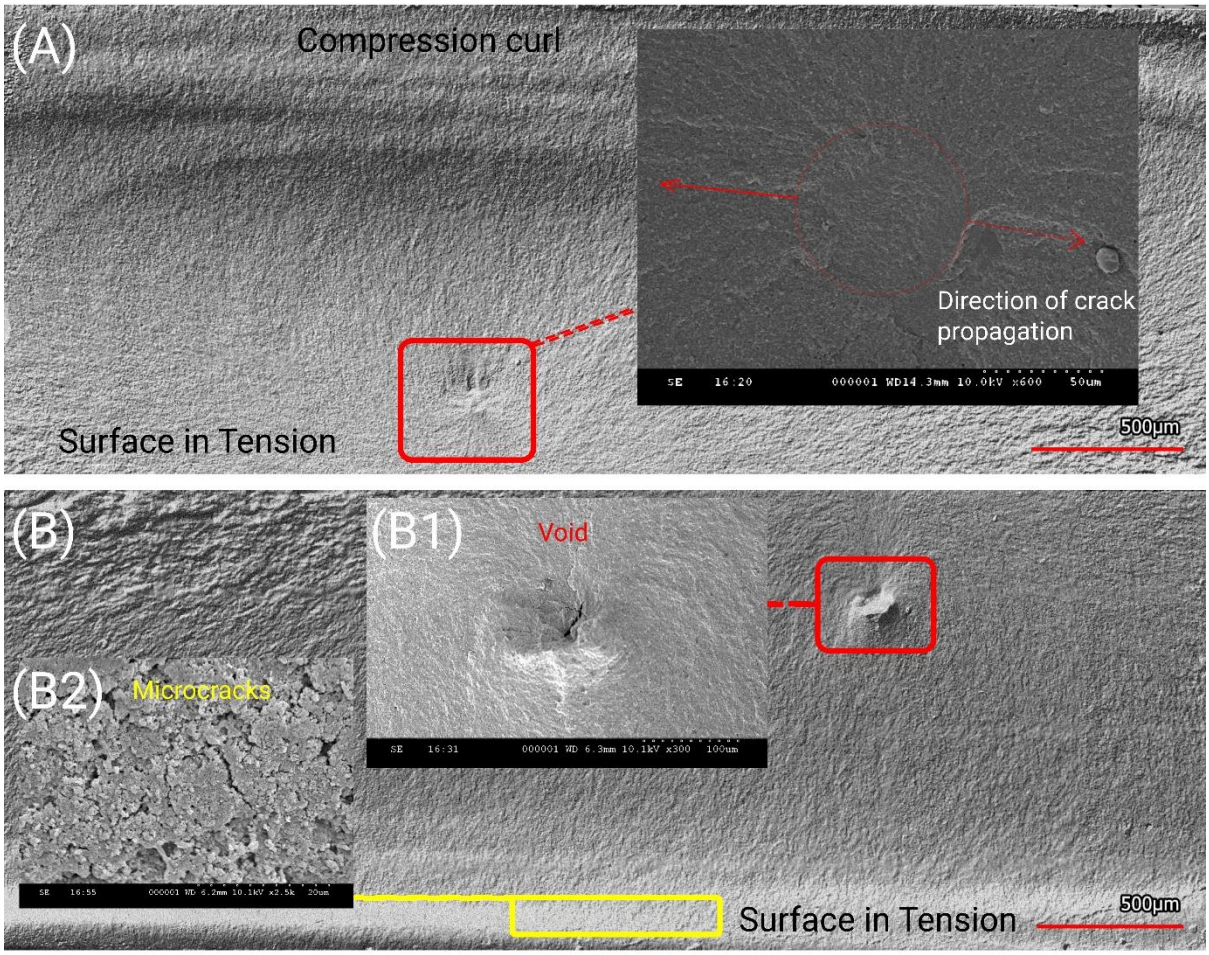

FIGURE 4

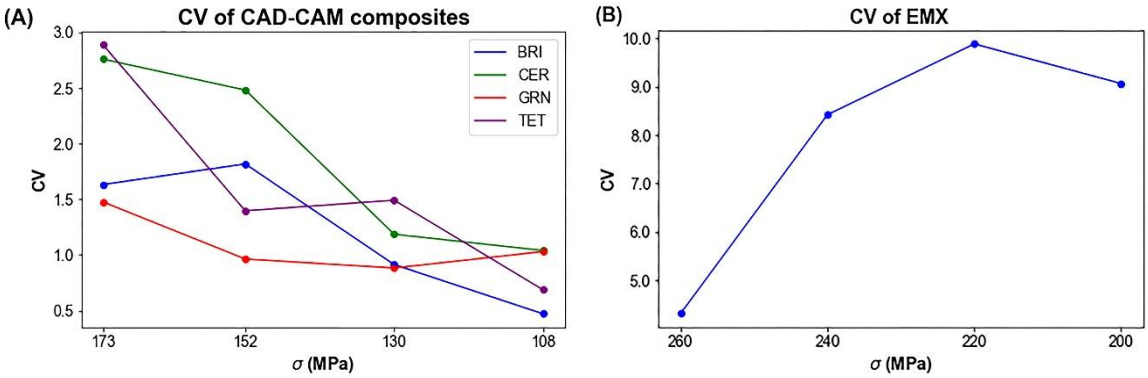
(A)
CV of CAD-CAM composites
BRI
CER
GRN
TET
CV
σ (MPa)
3.0
2.5
2.0
1.5
1.0
0.5
173
152
130
108
(B)
CV of EMX
CV
σ (MPa)
10.0
9.0
8.0
7.0
6.0
5.0
260
240
220
200

TABLE 1

Material (Abbreviation)	Manufacturer	LOT	Variants	Composition	
				Organic matrix	Inorganic fillers (filler content wt%)
Cerasmart 270 (CER)	GC, Tokyo, Japan	2102251 2204051	A1 HT 14	Bis-MEPP, UDMA, DMA	Barium glass (300 nm), silica (20 nm) (71wt%)
BRILLIANT Crios (BRI)	COLTENE, Altstätten, Switzerland	K81183 L80429	A2 LT 14	Methacrylates	Barium glass (<1 μm), SiO_2 (<20 nm) (71 wt%)
Tetric CAD (TET)	Ivoclar Vivadent, Italy	X09823 Z0Z0KK	A2 HT C14	Bis-GMA, Bis-EMA, TEGDMA, UDMA	Ba–Al–SiO_2-glass (<1μm), silica (<20nm), (71.1 wt%)
Grandio blocs (GRN)	VOCO GmbH, Cuxhaven, Germany	1806311 2145165	A2 HT 14L	UDMA + other DMA	Nanohybrid fillers, size of fillers unknown, (86 wt%)
IPS e.max CAD (EMX)	Ivoclar Vivadent, Schaan, Liechtenstein	Y02977 Z00447Y	A2 LT C14	-	Lithium disilicate glass-ceramics (LDS)

Data were completed according to manufacturers' information. Bis-GMA: bisphenol A glycol dimethacrylate; Bis-EMA: bisphenol A diglycidyl methacrylate ethoxylated; Bis-MEPP: bisphenol A ethoxylate dimethacrylate; TEGDMA: Triethylene glycol dimethacrylate; UDMA: Urethane dimethacrylate; SiO_2: Silicon oxide; Ba–Al–SiO_2: barium aluminium silicate glass.

TABLE 2

Materials	Mean FLS (SD)	m [90% CI]	σ_0 [90% CI]	FLS10	FLS50	FLS90
CER	214^{c}(30)	7.7$^{a, b}$ [5.6;10.6]	227.0^{c} [217.8;236.9]	170	216	253
BRI	218^{c} (25)	8.8$^{a, b}$ [6.4;12.0]	229.8^{c} [221.5;238.5]	178	220	252
TET	193^{d} (20)	10.6^{a} [7.7;14.5]	202.3^{d} [196.0;208.6]	163	195	219
GRN	247^{b} (26)	10.4^{a} [7.6;14.2]	258.5^{b} [251.4;267.7]	209	250	281
EMX	361 ^{a} (73)	4.9^{b} [3.4;7.2]	391.2^{a} [367.9;420.0]	249	363	462

FLS: flexural strength; Mean FLS (SD): average and standard deviation of FLS data; Weibull shape parameter (m), Weibull scale parameter σ_0, FLS10, FLS50, and FLS90: stress level where the likelihood of material failure is 10%, 50%, and 90%, respectively. For the Weibull modulus, the lack of overlap in the confidence interval is considered a statistical difference. Data in a column with different superscripts indicates statistical differences.

TABLE 3

Materials	173MPa		152MPa		130MPa		108MPa	
	N_0	m^*	N_0	m^*	N_0	m^*	N_0	m^*
BRI	$3.3x10^3$	0.64	$1.1x10^4$	0.58	$1.9x10^5$	1.09	$6.5x10^5$	2.24
CER	$5.1x10^3$	0.43	$1.1x10^4$	0.47	8.0x10	0.85	$1.4x10^6$	0.96
GRN	$1.2x10^4$	0.69	$1.9x10^4$	1.04	1.4x10	1.13	$1.3x10^6$	0.97
TET	$4.6x10^3$	0.42	$7.8x10^3$	0.73	$5.9x10^4$	0.69	$3.6x10^5$	1.48
	260MPa		240MPa		220MPa		200MPa	
	N_0	m^*	N_0	m^*	N_0	m^*	N_0	m^*
EMX	$2.8x10^3$	0.34	$1.6x10^4$	0.25	$2.3x10^4$	0.23	$6.7x10^5$	0.24

(N_0): The characteristics fatigue life (63.3%); m^*: The Weibull modulus of fatigue life.

TABLE 4

Materials	FAS/FLS ratio (5×10^4 cycles)	FAS (MPa) (2.5×10^5 cycles)	'n' [90% CI]
BRI	0.62	118.3	13.3 [9.5, 22.2][a]
CER	0.62	117.6	12.5 [9.3, 19.1][a]
GRN	0.57	120.6	10.9 [8.4, 15.6][a]
TET	0.65	108.6	10.4 [7.8, 15.9][a]
EMX	0.58	<200	14.2 [8.6,40.0][a]

Data in a column with different superscripts indicate that statistical analysis suggests significant differences. A material whose CI encompasses another material's point estimate is considered statistically similar.